Available online at www.sciencedirect.com
SCIENCE DIRECT®
Journal of Sound and Vibration 278 (2004) 307–326
JOURNAL OF SOUND AND VIBRATION
www.elsevier.com/locate/jsvi

Adaptive control of vibration wave propagation in cylindrical shells using SMA wall joint

M.B. Xu[a], G. Song[b,*]

[a] *Center for Automotive Research, The Ohio State University, Columbus, OH 43212, USA*
[b] *Department of Mechanical Engineering, University of Houston, Houston, TX 77036, USA*

Received 24 March 2003; accepted 6 October 2003

Abstract

A shape memory alloy (SMA) wall joint is proposed to adaptively attenuate and control the vibration wave propagation in cylindrical shells. A shape memory alloy wall joint inserted along the cylindrical shells acts as a source of mismatch of structural impedance with tunable characteristics. Thus, the SMA wall joint has the potential to solve the pass-band problem, which widely exists in the conventionally used wall joints. The performance of the SMA joint is attributed to a unique behavior of the shape memory alloy. That is, with the change of temperature, the Young's modulus of the SMA can be varied up to three times of its original value as the SMA undergoes a phase transformation from martensite to austenite. With such a tunable capability an SMA wall joint can introduce proper structural impedance mismatch at different frequency, which is necessary to attenuate and control the propagation of the incident vibration wave. Because the parameter of the SMA joint can be tuned adaptively, the incident wave with different frequencies can be highly attenuated and controlled. Therefore it has the potential to solve the problem of a pass-band existing in conventional wall joints. Numerical results demonstrate that the adaptive SMA wall joint with a proper temperature is able to control the vibration from a source with wideband frequencies or time-varying frequencies, and the transmission loss is more than 20 dB. The theoretical developments of the SMA joint in this paper provide guidelines for adaptive control of vibration wave propagation and the design of such tunable structures.

1. Introduction

Noise and vibration control finds wide applications in both domestic and industrial environments. In the field of duct noise control, the reactive method has been employed to

*Corresponding author. Tel.: +1-713-743-4525; fax: +1-713-743-4503.
E-mail address: gsong@uh.edu (G. Song).

0022-460X/$ - see front matter © 2003 Elsevier Ltd. All rights reserved.
doi:10.1016/j.jsv.2003.10.029

control the acoustic noise for a long time [1,2]. It attenuates noise by super-positioning sound waves of opposite signs so that positive air pressure is cancelled by negative air pressure. Expansion chambers and Helmholtz resonators are most commonly used in reactive mufflers. The performance of an expansion chamber is mainly determined by its geometrical shape. Usually, the performance is satisfactory only in a finite frequency range, however, a pass-band exists in the curve of the transmission loss (TL) as the noise is broadband. The existence of the pass-band problem can be interpreted in terms of the wave system inside a muffler. At very low frequencies or whenever the length of the muffler equals $\lambda(2n+1)/2$ where λ is the wavelength, $n = 1, 2, 3, \ldots$), a standing wave system is produced with enhanced sound pressure at the end walls of the cavity. This changes the characteristic impedance of the expansion chamber to the value for the inlet and outlet ducts. Therefore, at these resonance frequencies the muffler is a perfect impedance match for the duct and the transmission loss is 0 dB. Similar to the expansion chamber, a, Helmholtz resonator must be tuned precisely to achieve significant noise attenuation because the performance of a Helmholtz resonator is effective only in a very narrow frequency range. Changes in excitation frequency and environmental conditions greatly influence the performance of devices consisting of expansion chambers and Helmholtz resonators. In order to solve this problem, an adaptive passive system has been designed [3–6] through which the passive devices can be enhanced with on-board intelligence to tune parameters to ensure a robust performance in changing conditions. The principal advantage of such adaptive passive devices over purely passive solutions is that the devices remain tuned for changing environments and time-varying excitations.

Just as expansion chambers are widely employed to control duct noise, in the field of vibration control, various types of structural discontinuities are also employed to attenuate the structural wave propagation by introducing an impedance mismatch [7]. Cylindrical shell systems are widely used in many engineering applications, and machinery-induced vibration often occurs in them. Numerous methods have been developed to attenuate and control the vibration wave propagation in cylindrical shells. Among these methods, the wall joint is commonly used since it can effectively reflect the vibration energy associated with the incident wave and then reduce the amplitude of the transmitted vibration.

Harari [8,9] investigated the wave propagation in shells with a wall joint, and the related problem of travelling waves encountering a ring stiffener attached to the shell wall. The structural discontinuity considered in the papers consists of a spring-type insert and the results show high power reflection coefficients at the cut-on frequencies of various torsional waves. Fuller [10] has investigated the effects of discontinuities in the wall of a cylindrical shell on travelling flexural waves, and both the geometry and material discontinuities have been considered. Xu et al. [11] studied the performance of wall joints on the control of vibration wave, and the influences of the parameters of the wall joint on the transmission loss have been investigated. The stiffness and the length of the joint are found to be the key factors, which strongly influence the average value and the shape of the curve of the transmission loss. Furthermore, the wall joint was extended to control the structure–fluid coupled wave propagating in a fluid-filled cylindrical shell [12]. The transmission loss of the wall joint was studied and an analysis of power flow transmission and reflection was presented. Results demonstrated that both the material stiffness of the joint and the vibration frequency strongly influence the results. From their investigation, it is learned that wall joints with properly designed parameters can greatly attenuate the vibration wave propagation in

certain frequency ranges, but similar to the performance of an expansion chamber, a pass-band commonly exists in the curve of the transmission loss. This means that, at these frequency ranges, the incident vibration wave cannot be reflected and the vibration wave cannot be consequently attenuated. The existence of the pass-band is an inherent character of such wall joints, and boundary frequencies of the pass-band are mainly determined by the parameters of the wall joint. These parameters include length, wall thickness, Young's modulus and density of the material. The problem of the pass-band existence can be solved if these parameters of the wall joint can be tuned adaptively, just as the adaptive passive reactive muffler used in the field of duct noise control.

In fact, in the field of structural vibration control, such adaptive passive systems have also been employed. For instance, the vibration absorber is a commonly used element for passive control; and active and active/passive vibration absorbers have been developed [13,14]. Sun et al. [15] gave a survey of passive, adaptive and active tuned absorbers. In the field of smart materials and structures, various kinds of smart materials have been employed to control the structural vibration adaptively. Ruzzene and Baz [16,17] used shape memory alloy to control the vibration wave propagation in periodic composite rods. Chen et al. [18] used shape memory alloy inserts to control the longitudinal wave propagation along rods. These inserts act as sources of impedance mismatch with tunable characteristics. With such controllable capability, the inserts can introduce the proper impedance mismatch necessary to impede the wave propagation along the rods. Both experimental and theoretical results demonstrate the effectiveness and potential of the composites with tunable impedance mismatch sources in controlling wave propagation in rods. Mace et al. [19] investigated the net vibration transmission through two discontinuities in a one-dimensional waveguide system, and in particular through a structural insert. A tunable insert made of a magneto-rheological (MR) fluid-filled case is used, and the stop bands can be tuned.

In this paper, a shape memory alloy (SMA) wall joint is proposed to attenuate and control the wave propagation adaptively. The performance of the SMA joint is attributed to the unique behavior of the shape memory alloy [20]. That is, as the SMA undergoes a phase transformation from martensite to austenite, the Young's modulus of the SMA shell wall joint changes dramatically. With such a controllable property, the wall joint can introduce a proper impedance mismatch, which is necessary to effectively reduce the incident vibration wave at different frequencies. Since the Young's modulus of the SMA joint can be tuned adaptively according to the frequency of the incident vibration wave, the propagation parameters of the wall joint can be altered; as a result, the proper stiffness ratio between the wall joint and the base shell can be achieved according to frequency. Since the parameters of the SMA joint can be tuned adaptively, the incident wave with various frequencies can be highly attenuated and controlled. Therefore it has the potential to solve the problem of pass-band existing in a conventional wall joint. Numerical results demonstrate that the adaptive wall joint proposed in this paper is capable of controlling the vibration from a source with wideband or time-changing frequency. In practical engineering, the cylindrical shell is usually coupled with internally contained fluid and the conventional wall joint has already been employed to control its vibration [12]. In fact, the proposed SMA wall joint has the ability to effectively control the vibration transmission of such a fluid–shell coupled system. It is hoped that the proposed theoretical development of SMA joints with tunable characteristics will shed some light on the control of vibration wave propagation and the design of those structures.

The rest of the paper is organized as follows. Following this brief introduction of the SMA wall joint, the vibrational characteristics of an SMA cylindrical shell are investigated by the wave propagation approach in Section 2. Section 3 gives the concept of vibration power flow in the structure of the shell wall. Section 4 provides the analytic method of vibration wave control using a SMA joint. In Section 5, numerical analysis is provided for an SMA wall joint, and both the results of free wave propagation and the transmission loss are presented. Finally, the conclusions are presented in Section 6.

2. Wave propagation in a shape memory cylindrical shell

Prior to the investigation of the performance of the shape memory alloy wall joint on the vibration control, it is necessary to study the free wave propagation characteristics of such a structural element. The SMA wall is modelled as a thin-walled, elastic cylindrical shell which is shown in Fig. 1. The vibration motion of the shell can be described by the Flügge shell equations [21], which are expressed as

$$\mathbf{L}_j(u,\ v,\ w,\ \mu,\ \rho,\ E,\ R,\ h) = 0, \quad j = 1, 2, 3, \tag{1}$$

where $\mathbf{L}_j$ denotes differential operators; u, v and w are the shell displacements in the x, θ and r directions, respectively; μ, ρ and E are the Poisson ratio, the density and the Young's modulus of the shell material, respectively; R is the shell mean radius and h is the wall thickness.

The solution to Eq. (1), in a discrete form, can be expressed as

$$\begin{aligned} u(x,\theta) &= \sum_{s=1}^{4}\sum_{n=0}^{\infty} U_{ns}\cos(n\theta)\exp(\mathrm{i}\omega t - \mathrm{i}k_{ns}x + \mathrm{i}\pi/2),\\ v(x,\theta) &= \sum_{s=1}^{4}\sum_{n=0}^{\infty} V_{ns}\sin(n\theta)\exp(\mathrm{i}\omega t - \mathrm{i}k_{ns}x),\\ w(x,\theta) &= \sum_{s=1}^{4}\sum_{n=0}^{\infty} W_{ns}\cos(n\theta)\exp(\mathrm{i}\omega t - \mathrm{i}k_{ns}x), \end{aligned} \tag{2}$$

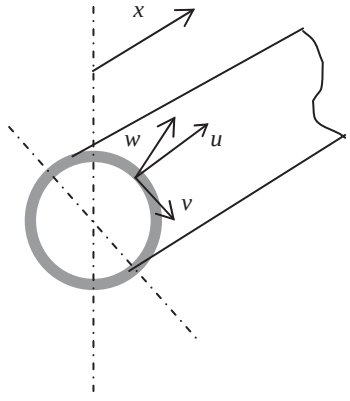

Fig. 1. Co-ordinate system and modal shapes.

where ω is radial frequency; k_{ns} is the axial wavenumber of mode (n,s); and U_{ns}, V_{ns} and W_{ns} are the amplitudes of the shell displacements.

Substituting of Eq. (2) into Eq. (1) results in the equations of motion in a symmetric matrix form

$$[L_{3\times3}]\begin{bmatrix} U_{ns} & V_{ns} & W_{ns} \end{bmatrix}^{\mathrm{T}} = \begin{bmatrix} 0 & 0 & 0 \end{bmatrix}^{\mathrm{T}}, \tag{3}$$

where all the elements of matrix L are functions of the non-dimensional $\lambda = k_{ns}R$ and non-dimensional frequency $\Omega = \sqrt{\rho R^2\omega^2(1-\mu^2)/E}$; and their expression are given in Appendix A. Expansion of the determinant of the amplitude coefficient in Eq. (3) provides the system characteristic equation,

$$A_1\lambda^8 + A_2\lambda^6 + A_3\lambda^4 + A_4\lambda^2 + A_5 = 0, \quad \text{for } n > 0 \tag{4a}$$

$$\left(B_1\lambda^6 + B_2\lambda^4 + B_3\lambda^2 + B_4\right) \times \left(e'\lambda^2 + f'\right) = 0 \quad \text{for } n = 0 \tag{4b}$$

with the coefficients $A_{1,2,3,4,5}$ and $B_{1,2,3,4}$ given in Appendix A. It can be seen that, for $n = 0$, the characteristic equation can be expressed as the product of two terms, indicating that the movement of the torsional waves is uncoupled with the movement of the bending/axial waves. The desired eigenvalues can then be obtained easily. For each circumferential modal number n, the wavenumber λ can be separated into two groups. The first group contains backward waves associated with the left semi-infinite shell $-\infty < x < 0$, excited at the edge at $x = 0$; the second group describes forward waves associated with the right semi-infinite shell, $0 < x < \infty$, excited at the edge at $x = 0$.

Substituting the roots back into Eq. (3) gives the characteristic vectors associated to the eigenvalues, which are expressed as

$$\Phi_{0s} = \frac{U_{0s}}{W_{0s}}, \quad \Psi_{0s} = 0 \quad \text{for } n = 0, \tag{5a}$$

$$\Phi_{ns} = \frac{U_{ns}}{W_{ns}} = \frac{L_{12}L_{23} - L_{13}L_{22}}{L_{11}L_{22} - L_{12}L_{21}}, \quad \Psi_{ns} = \frac{V_{ns}}{W_{ns}} = \frac{L_{21}L_{13} - L_{11}L_{23}}{L_{11}L_{22} - L_{12}L_{21}} \quad \text{for } n > 0, \tag{5b}$$

where the characteristic vectors Φ_{ns} and Ψ_{ns} characterize the particular type of wave motion, giving the ratio of the longitudinal and circumferential displacements to the flexural displacement. With the solutions of the wavenumber λ and the characteristic vectors Φ_{ns}/Ψ_{ns}, the characteristics of the vibration wave propagation in the SMA shell are can be obtained.

3. Vibration power flow in the shell wall

When there are propagating vibration waves in the shell wall, the vibration energy as well as the vibration motion will be transmitted along the shell in the axial direction with the propagation of the vibration wave. The vibration power flow along the shell axial direction can be expressed in the form of the shell internal force and the shell vibration velocity. When there is a wave (n,s) propagating along the shell wall in either positive or negative axial direction, there will be four types of forces in the shell wall in the axial direction. These forces for a particular circumferential

wavenumber n can be obtained as

$$\begin{aligned} N &= N_x \cos(n\theta)\mathrm{e}^{-\mathrm{i}k_{ns}x+\mathrm{i}\omega t} = N_{ns}W_{ns}\cos(n\theta)\mathrm{e}^{-\mathrm{i}k_{ns}x+\mathrm{i}\omega t},\\ T &= T_x \sin(n\theta)\mathrm{e}^{-\mathrm{i}k_{ns}x+\mathrm{i}\omega t} = T_{ns}W_{ns}\sin(n\theta)\mathrm{e}^{-\mathrm{i}k_{ns}x+\mathrm{i}\omega t},\\ S &= S_x \cos(n\theta)\mathrm{e}^{-\mathrm{i}k_{ns}x+\mathrm{i}\omega t} = S_{ns}W_{ns}\cos(n\theta)\mathrm{e}^{-\mathrm{i}k_{ns}x+\mathrm{i}\omega t},\\ M &= M_x \sin(n\theta)\mathrm{e}^{-\mathrm{i}k_{ns}x+\mathrm{i}\omega t} = M_{ns}W_{ns}\sin(n\theta)\mathrm{e}^{-\mathrm{i}k_{ns}x+\mathrm{i}\omega t}, \end{aligned} \tag{6}$$

where W_{ns} is the wave amplitude of the flexural displacement in the radial direction; N, T, S and M are the axial force, torsional shear force, transverse shear force and bending moment in the x direction, respectively; with their expressions provided in Appendix A.

In the shell wall at the section, the time averaged power flow for the propagating wave (n, s) transmitted by these forces are expressed as

$$\begin{aligned} P(n,s)_N &= \frac{1}{t}\int_0^t \int_0^{2\pi} N\left(\frac{\partial u}{\partial t}\right)^* R\,\mathrm{d}\theta\,\mathrm{d}\tau = 0.5\eta_n \pi R\,\mathrm{Re}\left[\mathrm{i}\omega N_x u^*\right]\\ P(n,s)_T &= \frac{1}{t}\int_0^t \int_0^{2\pi} T\left(\frac{\partial v}{\partial t}\right)^* R\,\mathrm{d}\theta\,\mathrm{d}\tau = 0.5\eta_n \pi R\,\mathrm{Re}\left[\mathrm{i}\omega T_x v^*\right]\\ P(n,s)_S &= \frac{1}{t}\int_0^t \int_0^{2\pi} S\left(\frac{\partial w}{\partial t}\right)^* R\,\mathrm{d}\theta\,\mathrm{d}\tau = 0.5\eta_n \pi R\,\mathrm{Re}\left[\mathrm{i}\omega S_x w^*\right]\\ P(n,s)_M &= \frac{1}{t}\int_0^t \int_0^{2\pi} M\left(\frac{\partial^2 w}{\partial x \partial t}\right)^* R\,\mathrm{d}\theta\,\mathrm{d}\tau = 0.5\eta_n \pi R\,\mathrm{Re}\left[\mathrm{i}\omega M_x \frac{\partial w^*}{\partial x}\right] \end{aligned} \tag{7}$$

where P_N, P_T, P_S and P_M are vibration power flow transmitted by different internal forces (N, T, S and M) in the shell wall; $t = 1/(2\pi\omega)$ being the period of the vibration

$$\eta_n = \begin{cases} 2 & \text{for } n = 0,\\ 1 & \text{for } n > 0, \end{cases}$$

and the asterisk $*$ denotes the complex conjugate.

The total power flow transmitted along the shell wall is the sum of the above four types of power flow expressed by Eq. (8), and is expressed as

$$P(n,s)_{total} = P(n,s)_N + P(n,s)_T + P(n,s)_S + P(n,s)_M. \tag{8}$$

4. Control of vibration wave propagation using SMA joint

A cylindrical base elastic shell with a wall joint made of SMA is shown in Fig. 2. Since the characteristics of the vibration wave are different between the base elastic shell and the SMA wall joint, the impedance mismatch can be introduced in the wave propagation guide if the SMA wall joint is inserted in a base elastic shell wall. As a result, the incident wave can be reflected by the impedance mismatch, and the vibration can be attenuated and localized. When there is a propagating wave which incidents from far left (in region a), the joint will reflect part of the

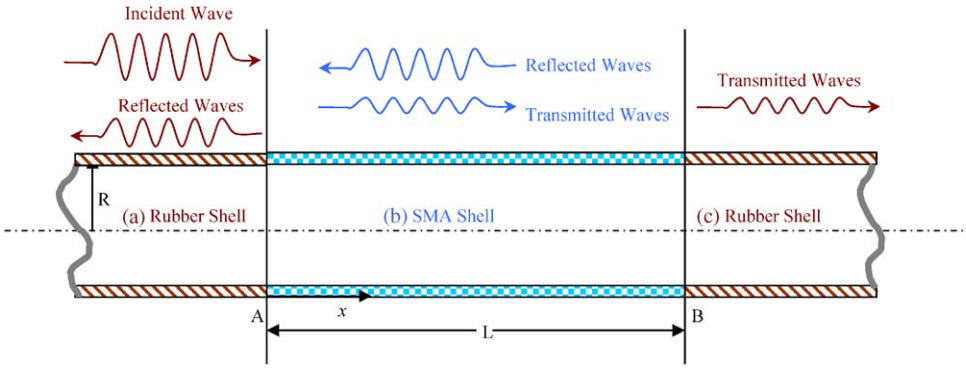

Fig. 2. An infinite cylindrical shell with a wall joint.

vibration energy associated with the incident wave, resulting in less energy carried by the transmitted wave in region (c) and in a reduced amplitude of the vibration wave transmitted from the wall joint. For the wall joint proposed in this paper, the vibration control is mainly due to the wave reflection caused by the mismatch of impedance, thus all local effects such as local stress concentrations are ignored. This approximation is justified by the initial assumption that the wall thickness is very small compared to the shell radius and the thickness parameter is retained only in flexural terms of the characteristic equation. In addition, SMA generally exhibits hysteretic behavior, which can be typically modelled by using a complex elastic modulus. However, in this paper, the dissipation caused by the hysteresis is neglected because of the assumption of small displacements and stress amplitudes. In addition, this small displacement/stress assumption implies also that the martensitic stress-induced transformation can be neglected. Thus, the material damping of the proposed SMA wall joint could be ignored in the analysis.

The performance of the SMA wall joint is analyzed by dividing the whole shell structure into three sections and considering wave propagation and reflection in each. For various values of circumferential mode n, the wave incidents on the joint is assumed to be the propagating wave $s = 1$ (s is shown in dispersion curves in Figs. 3–6, and $s = 1$ indicates the wave which has the lowest cut-on frequency). Commonly, a single incident wave of mode order $n > 0$ generates 4 reflected waves in region (a), 4 transmitted waves in wave (c), as well as 4 reflected and 4 transmitted waves in wave (b). Therefore there are a total of 16 generated waves with the identical mode order n ($n > 0$) and the same frequency. The number of boundary conditions (BC) at each discontinuity is 8. The boundary conditions include the continuities of angular bending velocity, radial, axial and tangential velocity; the continuities of angular bending moment, transverse shear, axial force and torsional shear force. Thus the total number of BC is also 16 for $n > 0$. For $n = 0$, because the torsional wave is uncoupled with the other waves, there are totally only 12 unknown waves, which include 3 reflected waves in region (a), 3 transmitted waves in wave (c), as well as 3 reflected and 3 transmitted waves in wave (b). At the interfaces A and B, there are 12 boundary conditions. Thus the number of the unknown amplitudes of these vibration waves is equal to the number of boundary conditions.

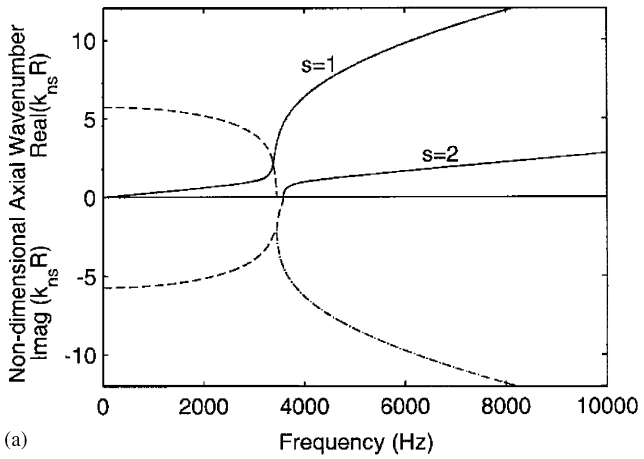

(a)

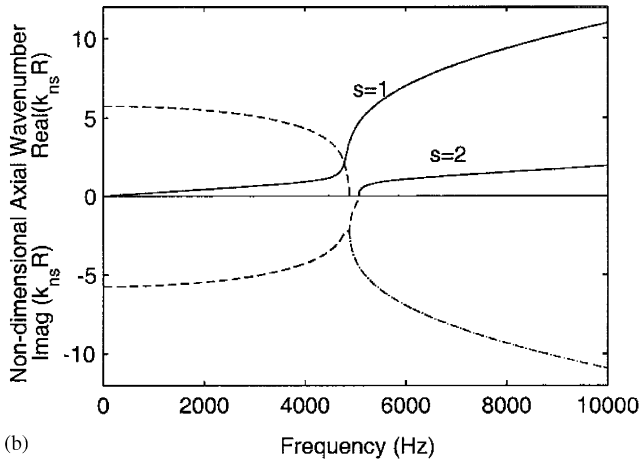

(b)

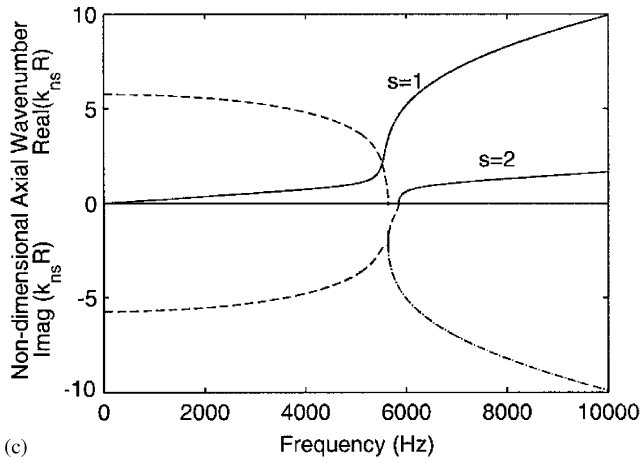

(c)

Fig. 3. Dispersion curves for a SMA shell at $n = 0$: (a) 25°C; (b) 48°C; (c) 70°C. —, propagating wave; ------, conjugate wave; –·–·–·–, near-field wave.

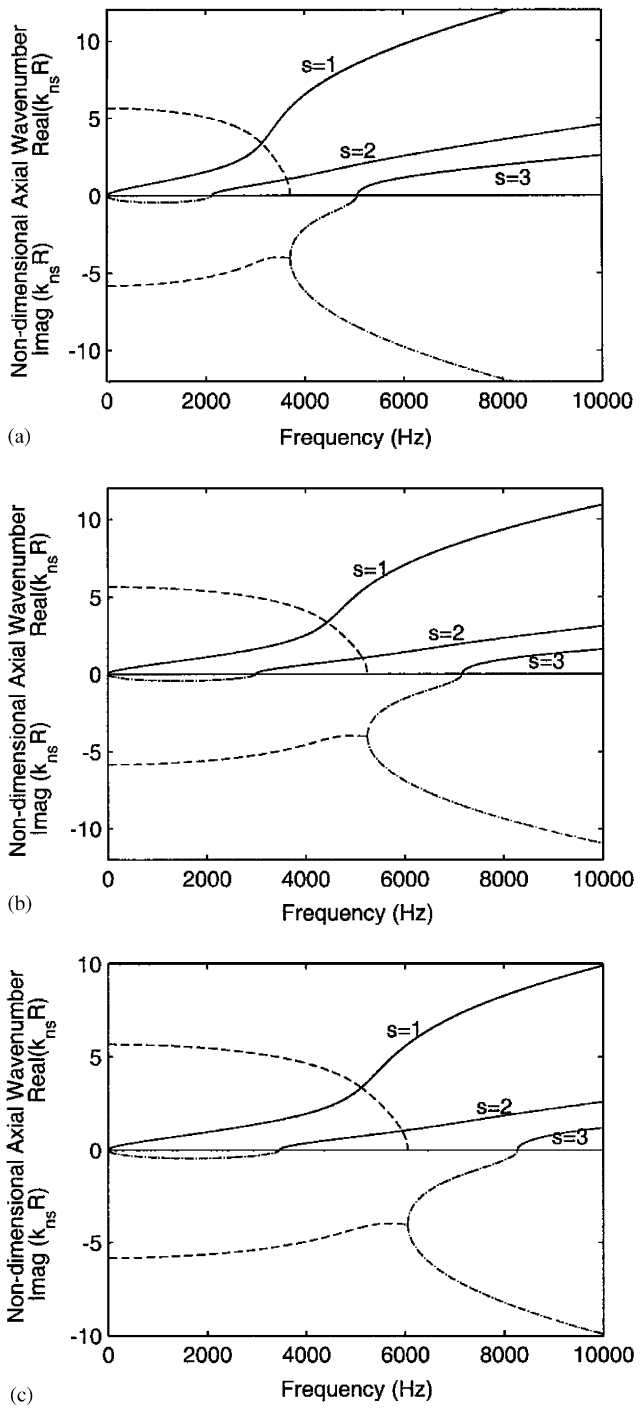

Fig. 4. Dispersion curves for SMA shell at $n = 1$: (a) 25°C; (b) 48°C; (c) 70°C. —, propagating wave; ------, conjugate wave; –·–·–·–, near-field wave.

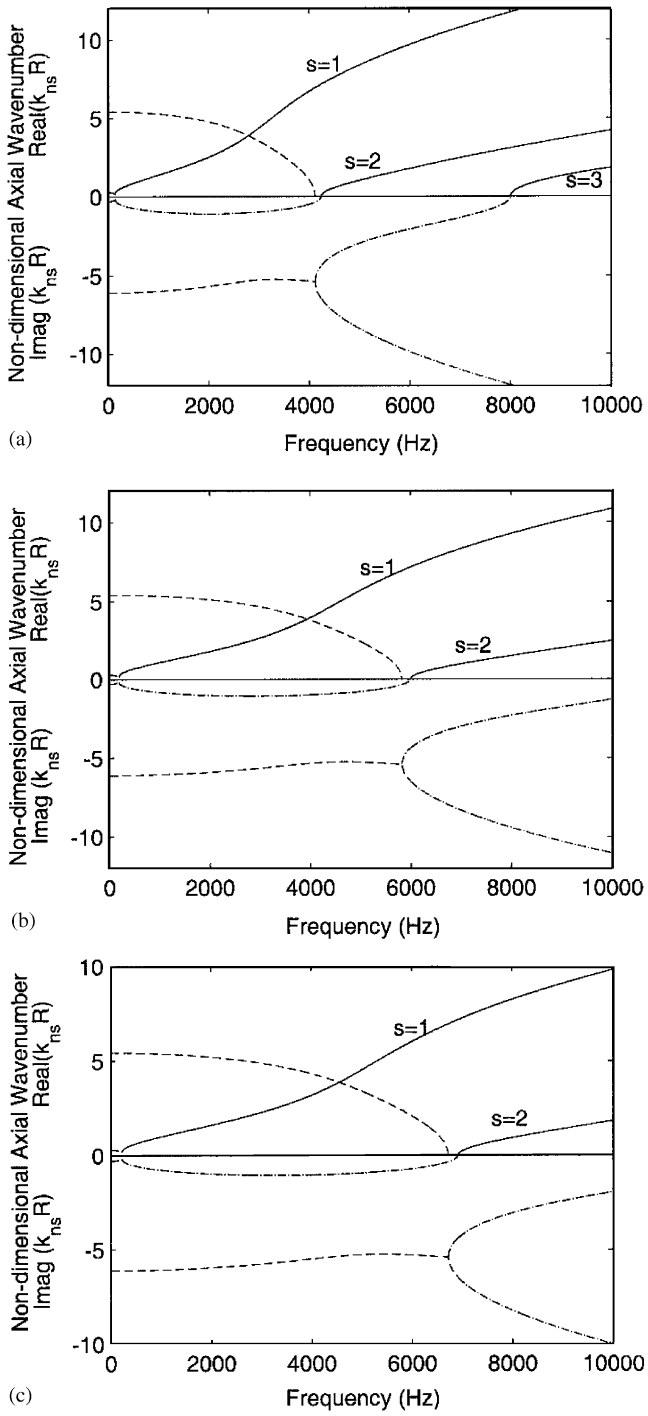

Fig. 5. Dispersion curves for SMA shell at $n = 2$: (a) 25°C; (b) 48°C; (c) 70°C. —, propagating wave; ------, conjugate wave; –·–·–·–, near-field wave.

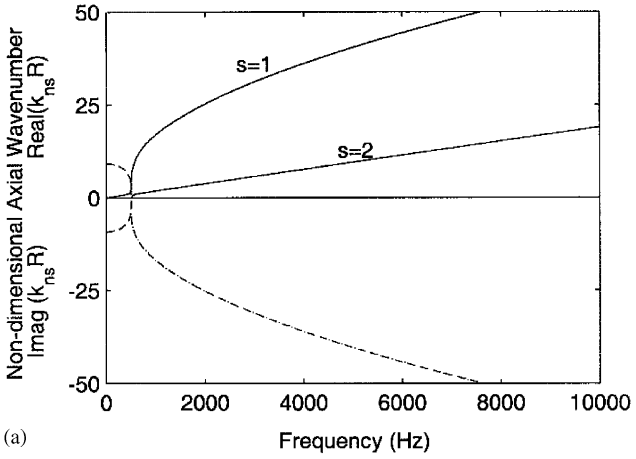

(a)

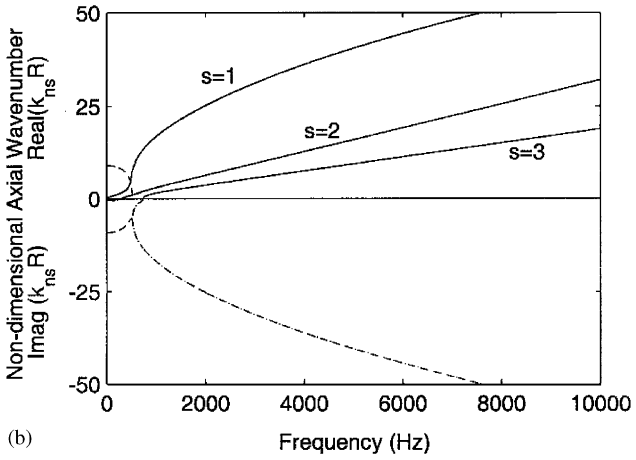

(b)

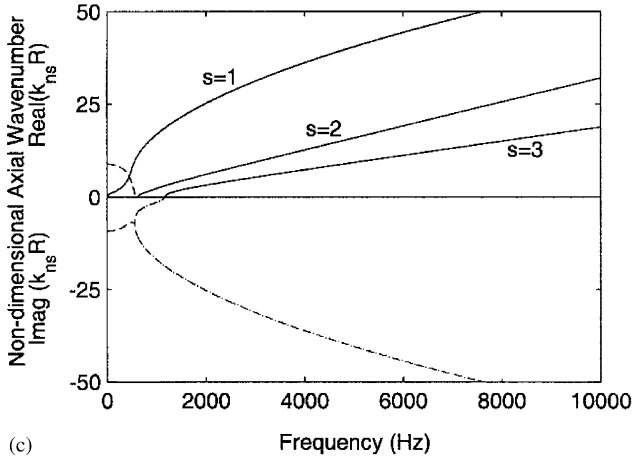

(c)

Fig. 6. Dispersion curves for a base elastic shell ($\rho = 2000\,\mathrm{kg/m^3}$, $E = 2 \times 10^8\,\mathrm{N/m^2}$, $\mu = 0.3$, $h/R = 0.02$ and $R = 0.1\,\mathrm{m}$): (a) $n = 0$; (b) $n = 1$; (c) $n = 2$. —, propagating wave; ------, conjugate wave; –·–·–·–, near-field wave.

At the interface A, for example, the continuity of radial velocity of the shell wall provides an equation, which is expressed as

$$\left(-W_{n1}^{ia}+\sum_{s=1}^{S}W_{ns}^{ra}\right)\Bigg|_{x=0}=\left(-\sum_{s=1}^{S}W_{ns}^{tb}+\sum_{s=1}^{S}W_{ns}^{rb}\right)\Bigg|_{x=0}, \tag{9}$$

where superscripts i, r and t refer to the incident wave, reflected waves and transmitted waves, respectively; a, b and c denote to the corresponding sections shown in Fig. 2; subscript n denotes the circumferential modal number and s denotes the axial branch number; $S=4$ for $n>0$ and $S=3$ for $n=0$. Similarly, by applying other boundary conditions, other equations can be provided and an equation group of size $4S$ will be obtained. The $4S$ unknown complex coefficients of the $4S$ equations were set into a matrix, and $4S\times 4S$ unknown Fourier amplitudes were then evaluated. Thus the main amplitudes of these considered waves in region (a), (b) and (c) could be obtained.

With the solution of the amplitudes of these vibration waves, the power flow carried by the incident wave, transmitted waves and reflected waves can be calculated and expressed as

$$P^{i}=P(n,1)_{total}^{ia},\quad P^{r}=\sum_{s=1}^{S}P(n,s)_{total}^{ra},\quad P^{t}=\sum_{s=1}^{S}P(n,s)_{total}^{tc}. \tag{10}$$

The transmission loss of vibration power flow (TL) is used to illustrate the performance of the wall joint, which is defined as

$$\begin{aligned}TL&=-10\log_{10}\left(\frac{\text{Power flow carried by the transmitted wave}}{\text{Power flow carried by the incident wave}}\right)\text{dB}\\&=-10\log_{10}\left(\frac{P^{t}}{P^{i}}\right)\text{dB}.\end{aligned} \tag{11}$$

In this paper, in order to check the results of the simulation, the principle of energy conservation is employed. That is, the energy associated with the incident wave P^{i} should be equal to the sum of the energies carried by the reflected waves P^{r} and that by the transmitted waves P^{t}, resulting in $P^{i}=P^{r}+P^{t}$. This principle is used to check the numerical simulation, and the accuracy of this method has been demonstrated by the example results.

As discussed in the introduction part, similarly to the pass-band problem existing for an expansion chamber-type muffler, this pass-band problem also exists for a conventionally used wall joint [10,12]. Thus the ability of vibration-wave control of such a wall joint is very poor in some frequency ranges. Since the frequency of the external disturbance is broad-range in practical engineering, the performance of this conventional wall joint must be improved. Generally, the boundary frequency of the pass-band is decided by the parameters of the wall joint (including the geometry of the wall joint and the material's characteristics of the joint), thus, an adaptive SMA wall joint proposed here can solve this problem. The performance of the adaptive wall joint is attributed to the unique behavior of the SMA. That is, as the SMA undergoes a phase transformation from martensite to austenite, the Young's modulus of the SMA shell wall joint can be varied up to about three times of its original value (the change of material parameters of SMA against the temperature is given in Table 1). With such a controllable capability, the wall joint can

Table 1
Properties of SMA wall joint at different temperatures

Temperature (°C)	Young's modulus (Pa)	Density (kg/m^3)	Poisson ratio
25	3e10	6500	0.3
48	6e10	6500	0.3
70	8e10	6500	0.3

introduce the proper impedance mismatch at different frequency, which is necessary for the joint to effectively control the incident vibration wave.

5. Numerical results

Numerical results are given for a base elastic shell with a SMA wall joint. The materials and geometry parameters of the base shell are: Young's modulus $E = 2.0 \times 10^8\ \mathrm{N/m^2}$, density $\rho = 2000\ \mathrm{kg/m^3}$, Poisson ratio $\mu = 0.3$, $h/R = 0.02$ and $R = 0.1$ m. The material parameters of the joint are given in Table 1 and the geometry parameters are: $h/R = 0.05$ and $R = 0.1$ m. The free wave propagation in the SMA cylindrical shell with different temperatures is studied and the transmission loss of this adaptive wall joint is then presented.

5.1. Characteristics of free wave propagation

In this part, the dispersion curves are presented for the SMA and base shell, and the characteristics of the dispersion curve are discussed. Generally, the dispersion curve gives the relationship between the non-dimensional wavenumber λ and the non-dimensional frequency Ω. However in this article, the dimensional frequency f (Hz) is employed instead of the non-dimensional frequency Ω. The reason is, for the SMA shell, that the same dimensional frequency f gives different values of the non-dimensional frequency Ω at different temperatures. Thus it is not convenient to discuss the influences of the temperature on the characteristics of free wave propagation. As a result, the relationships between the non-dimensional wavenumber λ and the dimensional frequency f are provided in this paper. The dispersion curves of the SMA shell at different temperatures are plotted in Figs. 3–5, the dispersion curves of base shell are given in Fig. 6. For the sake of brevity, neither the plot of characteristic vectors Φ_{ns}/Ψ_{ns} nor the discussions about the dispersion curves are provided here.

5.2. TL of adaptive SMA wall joint

The transmission loss (TL) of the adaptive wall joints on the incident propagating wave is discussed in this section, and the results are plotted against frequency f (Hz) in Fig. 7. Results with different circumferential wavenumber, length of the wall joint and the temperature of the wall joint are presented.

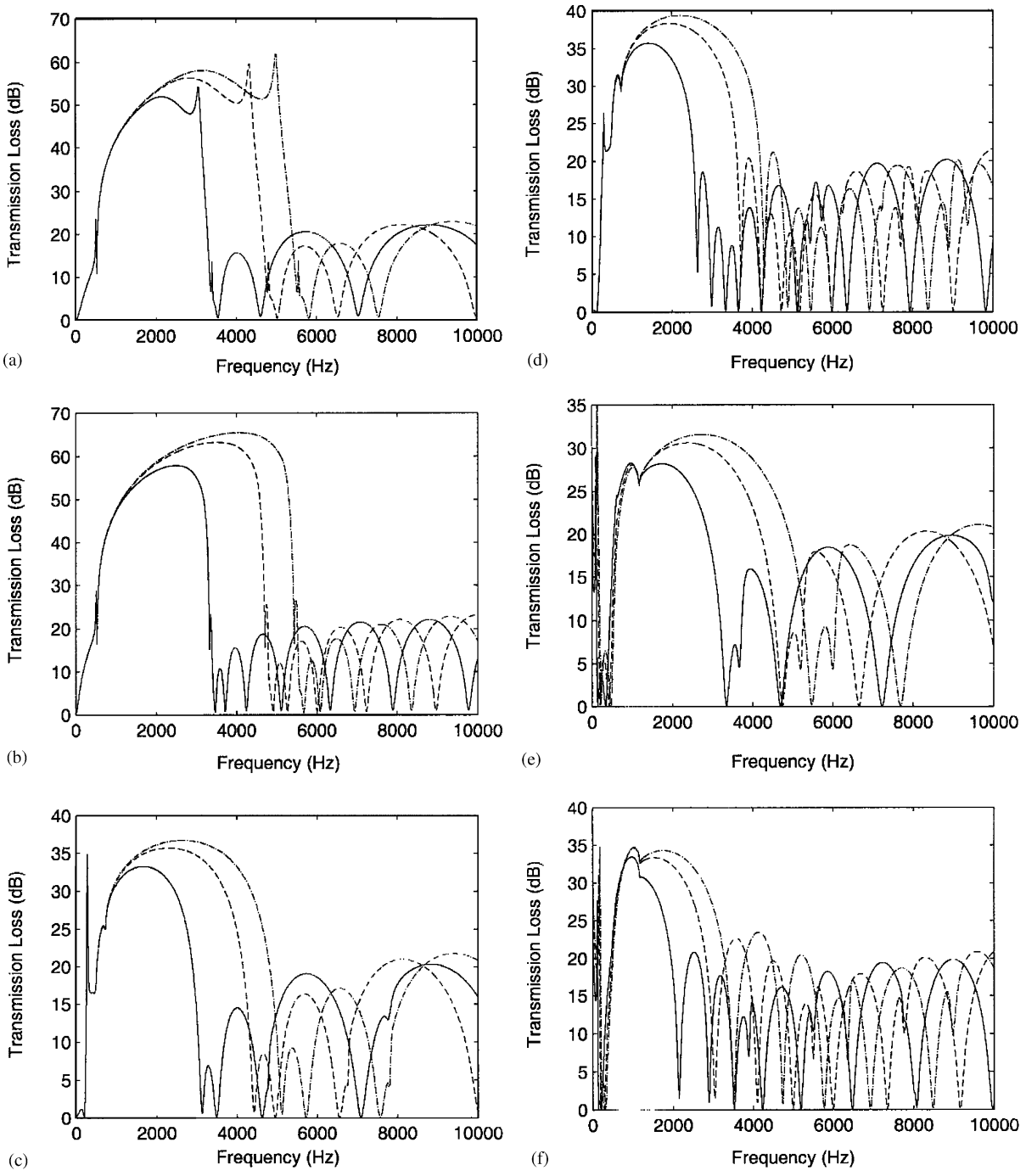

Fig. 7. Transmission loss of adaptive wall joint at different temperature: (a) $n = 0$, $L/R = 1$; (b) $n = 0$, $L/R = 2$; (c) $n = 1$, $L/R = 1$; (d) $n = 1$, $L/R = 2$; (e) $n = 2$, $L/R = 1$; (f) $n = 2$, $L/R = 2$. —, 25°C; - - - - -, 48°C; – · – · – · –, 70°C.

From the results, it can be conclude that, similar to the transmission loss of a muffler commonly used in the noise control field, there exist both pass-bands and stop-bands in the power spectral density (PSD) results of transmission loss of a wall joint with given length L and temperature T. The pass-band indicates that the TL is almost equal to zero in some frequency bands, which means that in these frequency bands, the energy carried by the input propagating wave cannot be controlled by the wall joint at all. The stop-band indicates that the input energy carried by the vibration wave can be effectively controlled by the wall joint. The existence of pass-bands means that the vibration problem of wideband or time-varying frequency cannot be solved by a conventional wall joint. However, with the capability of changing the PSD of TL, the adaptive wall joint has the potential to solve this problem.

5.2.1. Effect of wall joint length on the results

It can be concluded from the results that the length of the wall joint effectively changes the PSD of TL. With the increase of length, the number of the pass-bands and the stop-bands will increase, but the width of these bands will decrease. In practical engineering, the length of the wall joint cannot be easily changed according to the frequency of the input vibration wave, and the problem of the pass-band cannot be solved by altering the length of the wall joint. However, with the adaptive SMA wall joint proposed in this paper, this problem can be solved by altering the temperature with resulting in a changing value of Young's modulus. This is outlined below.

5.2.2. Effect of the temperature of SMA wall joint on the results

The material of the adaptive wall joint considered in this paper is SMA, which has many unique characteristics. One of the characteristics is that its Young's modulus varies up to several times of its original value as the SMA undergoes a phase transformation from martensite to austenite as its temperature increases. For example, in this case study, as the temperature changes from 25°C to 70°C, the Young's modulus of the SMA will change from 3×10^{10} to 8×10^{10} Pa. This characteristics can be employed to adaptively attenuate and control the wave propagation by regulating the SMA joint's temperature. From the results of earlier investigations [10–12], it is known that the Young's modulus has considerable effects on the results of TL. From the results in this paper, we see that the temperature has a great influence on the characteristics of the TL of the SMA wall joint. As the temperature changes, the number of the pass-bands and the stop-bands changes correspondingly. Furthermore, the boundary of the pass-band/stop-band and the location of the TL peak change as well. Take the case of $n = 0$ and $L/R = 1$, the following conclusions can be obtained from the results. For the temperature of 25°C, there are four stop-bands, which are about (0, 3500 Hz), (3500, 4700 Hz), (4700, 7000 Hz) and (7000–10000 Hz), the peak frequencies of TL are about 2000, 3100, 4000, 5700 and 8800 Hz. For the temperature of 48°C, there are three frequency bands, which are about (0, 5000 Hz), (5000, 6500 Hz) and (6500–10000 Hz), the peak frequencies of TL are about 3000, 4300, 5700 and 8000 Hz. For the case of 70°C, there are three bands, which are about (0, 5800 Hz), (5800, 7500 Hz) and (7500–10000 Hz), the peak frequencies of TL are about 3400, 5100, 6900 and 9400 Hz.

In practical engineering, this approach can be employed by the following steps. Firstly, the values of Young's modulus of the SMA at different temperature will be obtained to derive the relationship between Young's modulus E and temperature T, $E(T)$. Then, with the relationship between transmission loss TL and temperature T, $TL(T)$, the characteristics of TL (such as the

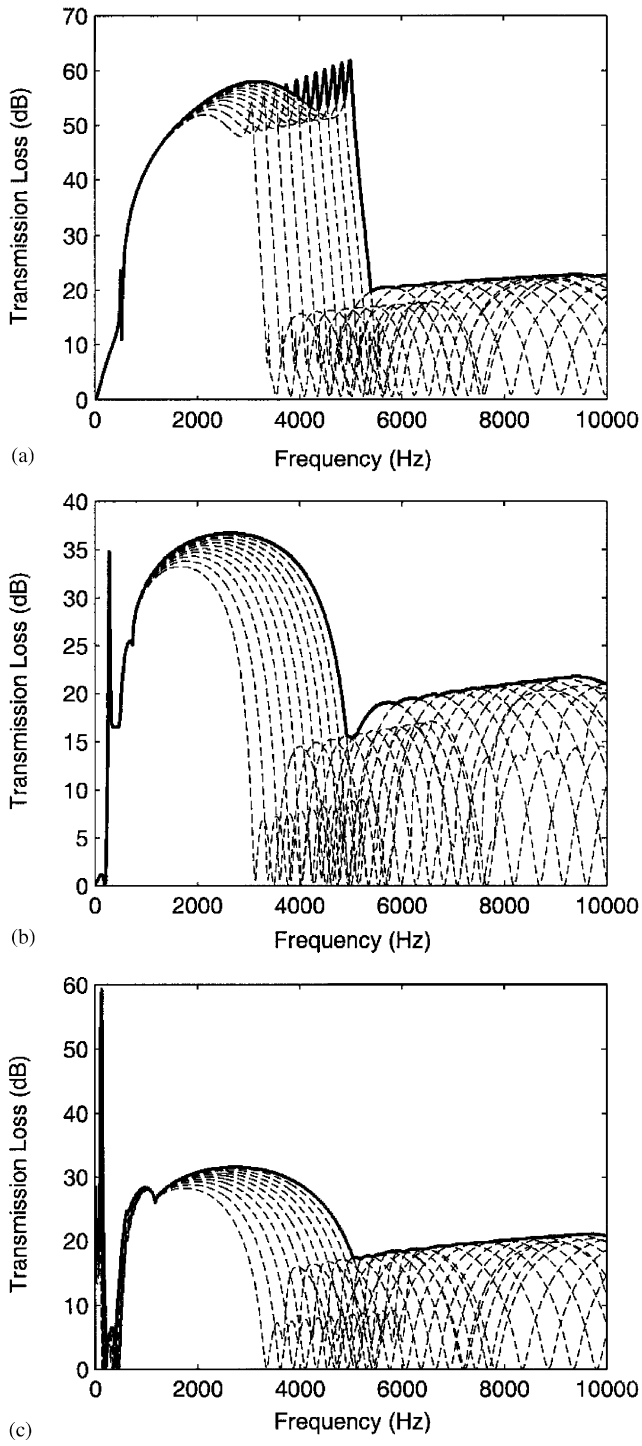

Fig. 8. Envelope line of TL of adaptive wall joint: (a) $n = 0$, $L/R = 1$; (b) $n = 1$, $L/R = 1$; (c) $n = 2$, $L/R = 1$. —, envelope line of TL; ------, TL of different temperatures.

boundaries of pass-bands and stop-bands, and the locations of the peak frequencies) at different temperature T will be known. Next, with the detecting of the peak frequencies of the power spectrum density of the vibration source, the critical frequencies, the peak frequencies of the TL, and the most suitable TL curve are determined. Finally the appropriate temperature for the SMA joint can be decided. In this way, the characteristics of the wall joint can be changed adaptively according to the vibration source, and the pass-band problem is then solved. For SMA, its Young's modulus can be any value in the range of $[3 \times 10^{10}, 8 \times 10^{10}\,\text{Pa}]$ depending on its temperature. The ideal TL value of the SMA wall joint should be the enveloping line of the TL curves at different temperatures. The results are provided in Fig. 8. For the case of $n = 0$, TL is above 50 dB for the frequency range of 0–5000 Hz, and is higher than 20 dB for frequencies above 5000 Hz; for $n = 1$, TL is above 30 dB for the range 0–4500 Hz and is about 20 dB for frequencies above 4500 Hz; for $n = 2$, TL is above 25 dB in the range of 0–4500 Hz and is about 20 dB for frequencies above 5000 Hz. From the above data, the proposed SMA wall joint has the potential to greatly improve the TL and solve the problem of pass-band.

6. Conclusions

In this paper, an innovative wall joint with adaptive characteristics is proposed. This adaptive wall joint is made of one kind of smart material, shape memory alloy, and the adaptive characteristics of such a wall joint are due to a unique property of SMA, that is, its Young's modulus can be altered by its temperature. This special property is employed to solve the pass-band problem associated with conventional wall joints. With such a controllable capability of SMA, the wall joint introduces a proper impedance mismatch for a particular frequency. This is necessary for the joint to reduce the incident vibration wave at that particular frequency. A case study and simulation results show that the adaptive wall joint has the ability of controlling the vibration source with wide-band frequencies or with a time-varying frequency. Numerical simulation indicates that the SMA wall joint has the potential to solve the problem of pass-band; and the transmission loss is more than 20 dB for all frequency ranges providing a proper temperature. The theoretical developments of the SMA joint in this paper provide guidelines for adaptive control of vibration wave propagation and the design of such tunable structures. However, the impact of damping of SMA material remains to be investigated in the future.

Appendix A. Force and moment resultants

The expression of matrix L in Eq. (3) is given as

$$[L_{3\times3}] = \begin{bmatrix} \lambda^2 + a' & b'\lambda & c'\lambda^3 + d'\lambda \\ & e'\lambda^2 + f' & g'\lambda^2 + h' \\ & & j' + k'\lambda^2 + l'\lambda^4 \end{bmatrix}, \tag{A.1}$$

with

$$a' = -(1-\mu)(1+K)n^2/2 + \Omega^2, \quad b' = (1+\mu)n/2, \quad c' = -K,$$
$$d' = \mu - K(1-\mu)n^2/2,$$
$$e' = -(1-\mu)(1+3K)/2, \quad f' = n^2 - \Omega^2,$$
$$g' = -(3-\mu)Kn/2, \quad h' = n,$$
$$j' = 1 + K(n^2-1)^2 - \Omega^2,$$
$$k' = -2n^2K, \quad l' = K, \quad K = h^2/(12R^2). \tag{A.2}$$

The expressions of coefficients $A_{1,2,3,4,5}$ and $B_{1,2,3,4}$ in Eq. (4) are

$$A_1 = e'l' - e'c'^2,$$
$$A_2 = e'k' + l'(f' + a'e') + 2b'g'l' - 2c'd'e' + f'c'^2 - g'^2 - b'^2l',$$
$$A_3 = e'j' + k'(f' + a'e') + a'f'l' + 2b'(g'd' + h'c') - (e'd'^2 + 2c'd'f') - (2g'h' + a'g'^2) - b'^2k',$$
$$A_4 = j'(f' + a'e') + a'f'k' + 2b'h'd' - f'd'^2 - (h'^2 + 2a'g'h') - b'^2j',$$
$$A_5 = a'f'j' - a'h'^2, \tag{A.3}$$

and

$$B_1 = l' - c'^2, \quad B_2 = k' + a'l' - 2c'd', \quad B_3 = a'k' - d'^2, \quad B_4 = a'j'. \tag{A.4}$$

In Eq. (6), the axial force, torsional shear force, transverse shear force, and bending moment in the x direction are expressed as

$$N_{ns} = D/R\left[\Phi_{ns}\lambda_{ns} + \mu n\Psi_{ns} + \mu - K\lambda_{ns}^2\right],$$
$$T_{ns} = D(1-\mu)/(2R)[-n\Phi_{ns} + (1+3K)\Psi_{ns}\lambda_{ns} + 3Kn\lambda_{ns}],$$
$$S_{ns} = DK/(2R)\left[(\lambda_{ns}^3 - \mu n^2\lambda_{ns} - \Phi_{ns}\lambda_{ns}^2 - \mu n\Psi_{ns}\lambda_{ns}) - (1-\mu)(2n^2\lambda_{ns} + 0.5n^2\Phi_{ns} + 1.5n\Psi_{ns}\lambda_{ns})\right],$$
$$M_{ns} = DK\left[\lambda_{ns}^2 - \mu n^2 - \Phi_{ns}\lambda_{ns} - \mu n\Psi_{ns}\right]. \tag{A.5}$$

Appendix B. Nomenclature

E	Young's modulus
f	frequency (Hz)
h	shell wall thickness
i	$\sqrt{-1}$

k	wavenumber
K	non-dimensional shell thickness
L	length of the wall joint
n	circumferential model number
N, T, S, M	shell internal force (moment)
P	power flow
s	branch number
t	$t = 1/(2\pi\omega)$, the period of the vibration
TL	transmission loss
u, v, w	shell displacements
x, r, θ	co-ordinates

Greek symbols

Φ, Ψ	eigenvector
μ	Poisson ratio
ρ	density
ω	circular frequency
Ω	non-dimensional frequency
λ	non-dimensional wavenumber

References

[1] D.D. Davis, G.M. Stokes, D. Moose, G.L. Stevens, Theoretical and Experimental Investigation of Mufflers with Comments on Engine-exhaust Muffler Design, NACA Report No. 1192, US Government Printing Office, Washington, DC, 1954.

[2] M.L. Munjal, *Acoustics of Ducts and Mufflers with Application to Exhaust and Ventilation System Design*, Wiley, New York, 1987.

[3] J.M. De Bedout, M.A. Franchek, R.J. Bernhard, L. Mongeau, Adaptive-passive noise control with self-tuning Helmholtz resonators, *Journal of Sound and Vibration* 202 (1997) 109–123.

[4] E. Little, A. Reza Kashani, J. Kohler, F. Morrison, Tuning of an electrorheological fluid-based intelligent Helmholtz resonator as applied to hydraulic engine mounts, in: R. Kashani (Ed.), *Transportation Systems*, ASME, New York, 1994, pp. 43–51.

[5] P. Krause, H. Weltens, S.M. Hutchins, Advanced exhaust silencing, *Automotive Engineering* 101 (1993) 13–16.

[6] H. Matsuhisa, B. Ren, S. Sato, Semiactive control of duct noise by a volume-variable resonator, *International Journal of the Japan Society of Mechanical Engineers* 35 (1992) 223–228.

[7] L. Cremer, M. Heckl, E.E. Ungar, *Structure-borne Sound*, 2nd Edition, Springer, Berlin, 1988.

[8] A. Harari, Wave propagation in a cylindrical shell with joint discontinuity, *Shock and Vibration Bulletin* 48 (1978) 53–61.

[9] A. Harari, Wave propagation in a cylindrical shell with finite region of structural discontinuity, *Journal of the Acoustical Society of America* 62 (1977) 1196–1205.

[10] C.R. Fuller, The effect of wall discontinuities on the propagation of flexural waves in cylindrical shells, *Journal of Sound and Vibration* 75 (1981) 207–228.

[11] M.B. Xu, X.M. Zhang, W.H. Zhang, The effect of wall joint on the power flow propagation in cylindrical shells, *Journal of Huazhong University of Science and Technology* 24 (1996) 72–75.

[12] M.B. Xu, X.M. Zhang, W.H. Zhang, The effect of wall joint on the vibrational power flow propagation in fluid-filled shell, *Journal of Sound and Vibration* 224 (1999) 395–410.
[13] K. Nagaya, A. Kurusu, S. Ikai, Y. Shitani, Vibration control of a structure by using a tunable absorber and an optimal vibration absorber under auto-tuning control, *Journal of Sound and Vibration* 228 (1999) 773–792.
[14] G. Lee, J. Gina, G. Ahmad, G.H. Lucas, Integrated passive/active vibration absorber for multistory buildings, *Journal of Structural Engineering* 123 (1997) 499–504.
[15] J.Q. Sun, M.A. Norris, M.R. Jolly, Passive, adaptive and active tuned vibration absorbers-a survey, *American Society of Mechanical Engineers, Journal of Vibration and Acoustics and Journal of Mechanical Design* 117 (1995) 234–242 (50th Anniversary).
[16] M. Ruzzene, A. Baz, Control of wave propagation in periodic composite rods using shape memory inserts, *Journal of Vibration and Acoustics* 122 (2000) 151–159.
[17] M. Ruzzene, A. Baz, Attenuation and localization of wave propagation in periodic rods using shape memory inserts, *Smart Materials and Structures* 9 (2000) 805–816.
[18] T. Chen, M. Ruzzene, A. Baz, Control of wave propagation in composite rods using shape memory inserts: theory and experiments, *Journal of Vibration and Control* 6 (2000) 1065–1081.
[19] B.R. Mace, R.W. Jones, N.R. Harland, Wave transmission through structure inserts, *Journal of the Acoustical Society of America* 109 (2001) 1417–1421.
[20] H. Funakubo, *Shape Memory Alloys*, Gordon and Breach, New York, 1987.
[21] W. Flügge, *Stress in Shells*, Springer, New York, 1973.